JOURNAL OF Materials CHEMISTRY

The crystal structure of a new oxide ion conductor $NaBi_3V_2O_{10}$ and oxide ion conductivity in $Pb_2Bi_2V_2O_{10}$

Derek C. Sinclair,[a] Eugenia Marinou[b] and Janet M. S. Skakle[b]

[a]*Department of Engineering Materials, University of Sheffield, Mappin Street, Sheffield, UK S1 3JD*
[b]*Chemistry Department, University of Aberdeen, Meston Walk, Aberdeen, UK AB24 3UE*

Received 27th May 1999, Accepted 3rd July 1999

Rietveld refinements using neutron diffraction data have been used to determine the crystal structure of the room temperature polymorph of a new oxide ion conductor, $NaBi_3V_2O_{10}$. The cell is isostructural with $Pb_2Bi_2V_2O_{10}$ and the data refined in spacegroup $P1$ with cell parameters of $a=7.0613(8)$, $b=7.2086(8)$, $c=5.5343(10)$ Å, $\alpha=113.328(4)$, $\beta=84.4787(14)$ and $\gamma=112.249(3)^\circ$ with an R value of 2.19%. The low symmetry of $Pb_2Bi_2V_2O_{10}$ and $NaBi_3V_2O_{10}$ is attributed to structural distortions associated with electron lone pairs on Pb^{+II} and Bi^{+III}. Replacement of Pb^{+II} by Bi^{+III} and Na^{+I} produces a structural phase transition to a higher symmetry polymorph in $NaBi_3V_2O_{10}$ at *ca.* 575 °C. ac Impedance measurements show $Pb_2Bi_2V_2O_{10}$ to be a modest oxide ion conductor with conductivity of *ca.* 1 mS cm^{-1} at 800 °C. As a result of the phase transition in $NaBi_3V_2O_{10}$ its conductivity is *ca.* one order of magnitude greater than that of $Pb_2Bi_2V_2O_{10}$ at 600 °C.

Introduction

Several bismuth vanadate phases are known to be good oxide ion conductors.[1–6] The high levels of conductivity are normally attributed to the presence of defect fluorite layers related to δ-Bi_2O_3, as in $Bi_{15}VO_{25}$[7] or with $Bi_2O_2^{2+}$ sheets interleaved with perovskite-like layers containing random oxide ion vacancies, as in $Bi_4V_2O_{11}$.[2] Recently we reported the synthesis and conductivity, σ, of a new oxide ion conductor, $NaBi_3V_2O_{10}$, with $\sigma=1$ mS cm^{-1} at 650 °C, which undergoes a reversible phase transition at *ca.* 575 °C and decomposes above *ca.* 700 °C.[8] Although the crystal structure was unknown, X-ray diffraction results showed the room temperature polymorph to be triclinic with $a=7.2026(10)$, $b=7.0600(9)$, $c=5.5312(6)$ Å, $\alpha=84.542(12)$, $\beta=113.318(11)$ and $\gamma=112.267(12)^\circ$. In an attempt to find an isostructural compound, a search was performed using the Crystal Data Identification File (CDIF)[9] using this unit cell. This gave the phase $Pb_2Bi_2V_2O_{10}$, space group $P1$, which has a similar stoichiometry and unit cell to that of $NaBi_3V_2O_{10}$. Brixner and Foris reported[10] that $Pb_2Bi_2V_2O_{10}$ retains the low triclinic symmetry up to the melting point of 895 °C.

The structure of $Pb_2Bi_2V_2O_{10}$ was determined by single crystal X-ray diffraction[11] and contains 2 Pb and 2 Bi sites which have distorted eight- and six-fold co-ordination, respectively. The distribution of Na and Bi between these four available sites in $NaBi_3V_2O_{10}$ was not known but theoretical X-ray diffraction patterns generated using the parameters from $Pb_2Bi_2V_2O_{10}$ matched well with the observed pattern when Na was located on either the Pb(1) or Bi(2) site. Full Rietveld refinement using the powder X-ray data was not attempted due to the complexity of the structure. In addition, Bi atoms dominate the X-ray scattering in this structure and therefore the oxygen atoms are difficult to locate accurately, which is a particular problem given the interest in this material as an oxide ion conductor. In contrast, neutron diffraction data should overcome both these problems and permit structure determination.

In a study of $Pb_2Bi_2V_2O_{10}$, Wang and Li[11] compare the structure of $Pb_2Bi_2V_2O_{10}$ to that of Lanarkite,[12] $PbO{\cdot}PbSO_4$ which is based on the defect fluorite structure of red PbO. Given that oxide ion conductivity is a common occurrence in many defect fluorites, this may explain the origin of oxide ion conduction in $NaBi_3V_2O_{10}$ and suggests that $Pb_2Bi_2V_2O_{10}$ may also be an oxide ion conductor. In this paper we report neutron diffraction data on the room temperature crystal structure of $NaBi_3V_2O_{10}$ and electrical conductivity measurements on $Pb_2Bi_2V_2O_{10}$.

Experimental

$NaBi_3V_2O_{10}$ and $Pb_2Bi_2V_2O_{10}$ were prepared by solid state reaction of Bi_2O_3 (99.99%), V_2O_5 (99.6%), Na_2CO_3 (99.99%) and PbO (99.9%). Stoichiometric quantities of the appropriate reagents were ground together with acetone in an agate mortar and pestle, dried, placed in Au boats and fired at 600 °C for 24 h. To obtain single phase samples, experience showed the regrinding and refiring process had to be repeated twice at 650 °C for $NaBi_3V_2O_{10}$ and twice at 800 °C for $Pb_2Bi_2V_2O_{10}$. Sample purity was checked by a combination of X-ray diffraction and Electron Probe Micro-Analysis (EPMA), as described elsewhere.[8,13]

Powder neutron diffraction data for $NaBi_3V_2O_{10}$ were collected on the Polaris diffractometer at the UK spallation neutron source ISIS, Rutherford Appleton Laboratory. Rietveld refinement was carried out using the program TF14LS,[14,15] with data collected over the time-of-flight range 4000–19 520 μs in the highest resolution, back-scattering detectors. The normalised neutron diffraction patterns were corrected for sample absorption effects.[15] Scattering lengths of 3.63(2), 8.532(2), −0.3824(12) and 5.803(4) fm, for Na, Bi, V and O, respectively, were taken from Sears.[16]

Pellets of $Pb_2Bi_2V_2O_{10}$ for ac impedance measurements were cold pressed in a 13 mm die under a pressure of ≈2 MPa prior to sintering at 850 °C in air for 12 h. Gold electrodes were applied to the major faces of sintered pellets by a combination of Au foil and organogold paste which was hardened at 800 °C. The electroded samples were mounted in an impedance jig and placed in a tube furnace where the temperature was controlled to ±3 °C over the range 25–800 °C. ac Impedance measurements were carried out between 5 Hz and 13 MHz

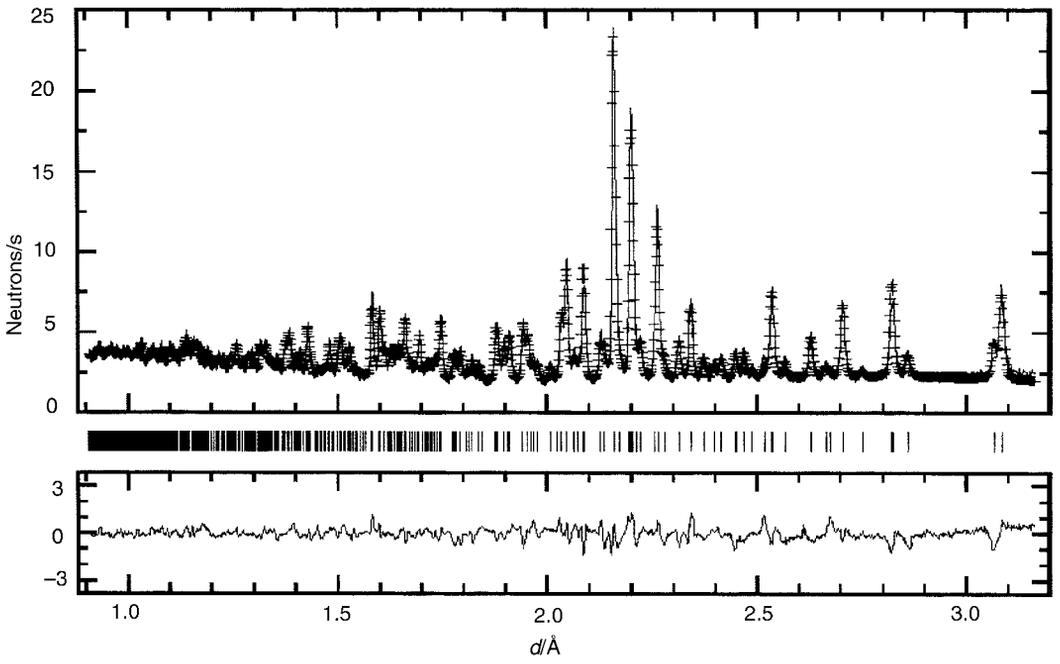

Fig. 1 Neutron diffraction pattern and difference profile of $NaBi_3V_2O_{10}$ after refinement.

using a Hewlett-Packard 4192A Impedance Analyser and between 10^{-2} Hz and 65 kHz using combined 1250/1287 Solartron instrumentation with an applied voltage of 100 mV. Data were collected on a heating and cooling cycle between 25 and 880 °C and corrected for sample geometry and for a measured jig parallel capacitance of 4 pF.

Results and discussion

EPMA results showed no evidence of any secondary phases on a μm scale for $NaBi_3V_2O_{10}$ or $Pb_2Bi_2V_2O_{10}$. Quantitative EPMA analysis determined the compositions to be 15.9(5) mol% Na_2O, 33.6(2) mol% V_2O_5 and 50.5(3) mol% Bi_2O_3 for $NaBi_3V_2O_{10}$, and 33.3(3) mol% PbO, 33.3(2) mol% V_2O_5 and 33.3(3) mol% Bi_2O_3 for $Pb_2Bi_2V_2O_{10}$. These results are in good agreement with the starting compositions.

Starting parameters for the refinement of $NaBi_3V_2O_{10}$ were taken from $Pb_2Bi_2V_2O_{10}$, using the unit cell determined from powder X-ray data.[10] Vanadium is effectively transparent to neutrons, so these positions were fixed. In addition, the Bi(2) site was fixed to define the origin; this site was chosen as the theoretical patterns suggested that it did not contain Na. In the initial refinements an average scattering length of 7.306 fm was used for the non-vanadium cations and the site occupancies refined so that the correct site for Na could be deduced. All oxygen thermal parameters were constrained to be the same, as were those for the two vanadium atoms and for the other four cations.

The site occupancy refinements for the non-vanadium cations converged to values between 1.1 and 1.2 for the first three sites and to 0.54 for the fourth site, indicating that Na was located on this fourth site. Refinement thus proceeded using this site assignation and the correct scattering lengths, and converged to give a final R value of 2.19%, $\chi^2 = 11.352$. Given the large number of variables, no attempt was made to refine the oxygen site occupancies. The final atomic coordinates are given in Table 1, bond lengths in Table 2 and the fitted neutron diffraction profile is shown in Fig. 1. Bond valence sums for $NaBi_3V_2O_{10}$ were calculated from the bond lengths using appropriate constants from Brown and Altermatt[17] and are given in Table 2, together with bond valence sums for $Pb_2Bi_2V_2O_{10}$ calculated from the reported bond lengths.[11]

The average bond lengths for the cations in $NaBi_3V_2O_{10}$, Table 2, are in good agreement with typical values for Bi^{+III}–O, Na^{+I}–O and V^{+V}–O distances, although considerable distortion is evident in all polyhedra. The irregular eight-fold co-ordination of Bi(1) and Bi(2) with the presence of long, *e.g.* >2.8 Å, and short bonds, *e.g.* <2.2 Å, is typical of a lone-pair cation such as Bi^{+III}. Bond valence sums for Bi and V are low and that of Na high. Considering the complexity of the structure, these values are consistent with the site assignation deduced from the refinements; however, they may also suggest some disorder of Na and Bi ions on the Na and Bi sites. Those of $Pb_2Bi_2V_2O_{10}$ are given as comparison; again, the values are not wholly conclusive and, in particular, the valence sum for Pb(1) is very high, which may indicate incorrect site assignment(s). Pb^{+II} and Bi^{+III} are both lone electron pair cations of similar size and therefore likely to occupy similar sites within the structure. The reported Pb and Bi site assignments in $Pb_2Bi_2V_2O_{10}$ should be treated with caution as the structure was determined by single crystal X-ray diffraction where Pb and Bi cannot be distinguished due to the similarity in their scattering factors.

The structure of $NaBi_3V_2O_{10}$ is shown in Fig. 2. The VO_4 tetrahedra are isolated; each Bi(1) links with two V(1)O_4

Table 1 Final refined parameters for $NaBi_3V_2O_{10}$; space group $P\bar{1}$ (no. 1), $a = 7.0613(8)$, $b = 7.2086(8)$, $c = 5.5343(10)$ Å, $\alpha = 113.328(4)$, $\beta = 84.4787(14)$ and $\gamma = 112.249(3)°$

Atom	*x/a*	*y/b*	*z/c*	B_{iso}
Bi1	0.6188(21)	0.6650(20)	0.252(3)	1.55(7)
Bi2	0.8529(-)	0.2718(-)	0.6059(-)	1.55(7)
Bi3	0.9990(20)	0.9950(20)	0.994(3)	1.55(7)
Na	0.470(3)	0.925(3)	0.885(4)	1.55(7)
V1	0.0816(-)	0.6136(-)	0.2632(-)	0.40(8)
V2	0.3906(-)	0.3100(-)	0.5927(-)	0.40(8)
O1	0.005(3)	0.332(3)	0.103(4)	1.63(9)
O2	0.424(3)	0.573(3)	0.780(4)	1.63(9)
O3	0.330(3)	0.793(3)	0.323(3)	1.63(9)
O4	0.115(3)	0.092(3)	0.460(3)	1.63(9)
O5	0.985(3)	0.678(3)	0.058(3)	1.63(9)
O6	0.553(3)	0.242(3)	0.805(4)	1.63(9)
O7	0.908(3)	0.642(3)	0.528(3)	1.63(9)
08	0.444(3)	0.255(3)	0.309(4)	1.63(9)
O9	0.716(3)	0.949(3)	0.169(4)	1.63(9)
O10	0.714(3)	0.972(3)	0.664(4)	1.63(9)

Note: all atoms are in 1-fold Wyckoff positions.

tetrahedra to form infinite chains in the *a* direction. Similarly, each Bi(2) links to two $V(2)O_4$ tetrahedra to form infinite chains in the same direction. Each Bi(1) and Bi(2) within these chains also connects to an adjacent $V(2)O_4$ and $V(1)O_4$, respectively to form 'double $BiVO_4$-type chains' in the *a* direction, as illustrated by the filled bonds between the atoms in Fig. 2(a). Each 'double $BiVO_4$-type chain' is linked by Bi(1) and Bi(2) atoms which connect *via* O(9) and O(10), as illustrated by the unfilled bonds between the atoms in Fig. 2(a). Presumably the lone electron pairs associated with Bi(1) and Bi(2) protrude into the voids within the 'double chains' and are responsible for the low symmetry in $NaBi_3V_2O_{10}$. Bi(3) and Na each have irregular six-fold co-ordination which is omitted from Fig. 2(a) for the sake of clarity. In terms of space filling polyhedra, Bi(1)–O_8 and Bi(2)–O_8 have common edges, O(9) and O(10), which connect with distorted Bi(3)–O_6 and Na–O_6 octahedra and extend along the *bc* plane.

By analogy with $PbO{\cdot}PbSO_4$, the formula $NaBi_3V_2O_{10}$ may be rewritten as $[(Na_{1/2}Bi_{1/2})O]{\cdot}[BiVO_4]$ and oxide ion conduction may occur in the regions between the 'double $BiVO_4$-type layers' which contain Bi and Na ions in highly distorted environments, Fig. 2(b). Unfortunately, the low symmetry of the structure makes it difficult to identify the presence of any obvious conduction planes, such as defect fluorite layers. Electron spin resonance (ESR) spectroscopy did not reveal the presence of any V^{4+} (d^1) in $NaBi_3V_2O_{10}$ suggesting that there is no significant oxygen non-stoichiometry in this compound. Further studies to determine the structure of the high temperature polymorph are in progress in an attempt to understand how oxygen ion migration occurs in $NaBi_3V_2O_{10}$.

ac Impedance measurements were conducted on a sintered pellet of $Pb_2Bi_2V_2O_{10}$ coated with Au electrodes. Complex impedance plane, Z^*, plots consisted of a single, semi-circular arc and a low frequency electrode 'spike', as shown in Fig. 3. The associated capacitance of the arc was calculated to be *ca.* 2–3 pF cm^{-1} using the relationship $\omega RC = 1$ (where $\omega = 2\pi f$ and f is the applied frequency) at the arc maximum. This value was temperature independent over the measured range and is consistent with a bulk or intra-granular response.[18]

The presence of a low frequency spike with an associated capacitance of 1–2 μF cm^{-1} in Fig. 3 is attributable to ionic polarisation and diffusion-limited phenomena at the electrode and supports the idea that the conduction in $Pb_2Bi_2V_2O_{10}$ is mainly by means of ions. A similar Warburg-type response was observed for $NaBi_3V_2O_{10}$ where the oxygen partial pressure at

Table 2 Bond lengths and bond valence sums for (a) $NaBi_3V_2O_{10}$ and (b) $Pb_2Bi_2V_2O_{10}$. BL = bond length in Å, BV = bond valence, BVS = bond valence sum

(a)		BL/Å	BV	(b)		BL/Å	BV
Bi1	O2	2.79	0.19	Pb1	O2	2.61	0.27
	O3	2.48	0.35		O3	2.39	0.46
	O5	2.69	0.23		O5	2.71	0.22
	O6	2.97	0.14		O6	3.02	0.11
	O7	2.75	0.21		O7	2.74	0.20
	O8	2.87	0.17		O8	2.95	0.13
	O9	2.12	0.77		O9	2.32	0.55
	O10	2.39	0.42		O10	2.23	0.70
BVS			2.46	BVS			2.64
Bi2	O1	2.86	0.171	Pb2	O1	2.71	0.22
	O4	2.54	0.310		O4	2.39	0.46
	O5	2.88	0.166		O5	2.93	0.14
	O6	2.27	0.544		O6	2.38	0.47
	O7	2.75	0.209		O7	2.78	0.19
	O8	3.02	0.131		O8	3.13	0.09
	O9	2.55	0.306		O9	2.57	0.30
	O10	2.15	0.716		O10	2.48	0.37
BVS			2.553	BVS			2.24
Bi3	O1	2.24	0.58	Bi1	O1	2.28	0.53
	O4	2.52	0.32		O4	2.52	0.32
	O5	2.41	0.40		O5	2.39	0.42
	O7	2.72	0.22		O7	2.94	0.15
	O9	2.10	0.80		O9	2.24	0.58
	O10	2.76	0.20		O10	2.38	0.43
BVS			2.52	BVS			2.43
Na1	O2	2.26	0.26	Bi2	O2	2.41	0.40
	O3	2.90	0.06		O3	2.59	0.28
	O6	2.34	0.21		O6	2.40	0.41
	O8	2.65	0.11		O8	2.79	0.19
	O9	2.37	0.20		O9	2.13	0.75
	O10	2.01	0.45		O10	2.22	0.61
BVS			1.29	BVS			2.64
V1	O1	1.742	1.152	V1	O1	1.77	0.94
	O3	1.707	1.276		O3	1.69	1.26
	O5	1.666	1.440		O5	1.64	1.47
	O7	1.816	0.926		O7	1.67	1.34
BVS			4.794	BVS			5.01
V2	O2	1.696	1.318	V2	O2	1.70	1.23
	O4	1.960	0.607		O4	1.83	0.84
	O6	2.019	0.510		O6	1.83	0.84
	O8	1.507	2.299		O8	1.64	1.47
BVS			4.734	BVS			4.38

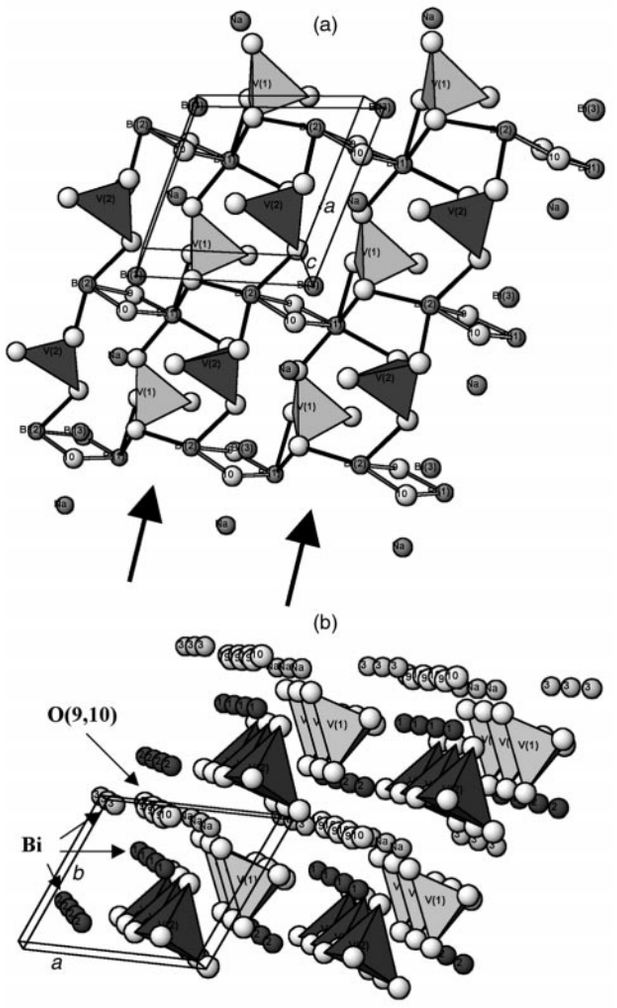

Fig. 2 Projections of the $NaBi_3V_2O_{10}$ crystal structure. In (a), 9 and 10 represent O(9) and O(10), respectively.

the electrode/$NaBi_3V_2O_{10}$ sample interface was found to have a dramatic effect on the low frequency response, indicating that conduction was mainly *via* O^{2-} ions.[8] Similar behaviour was observed for $Pb_2Bi_2V_2O_{10}$ suggesting that this material is also predominantly an O^{2-} ion conductor. Ion blocking measurements are in progress to quantify the oxide ion transport number in $NaBi_3V_2O_{10}$ and $Pb_2Bi_2V_2O_{10}$.

Bulk conductivity values were calculated from the reciprocal of the low frequency intercept of the semi-circular arc with the Z' axis of Z^* plots and are shown in the form of an Arrhenius

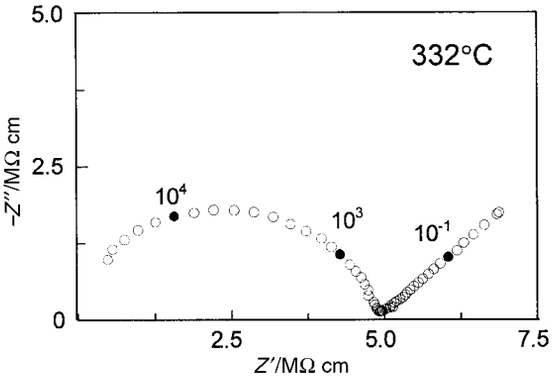

Fig. 3 The Z^* plot for $Pb_2Bi_2V_2O_{10}$ in air at 332 °C. Selected frequencies in filled circles are defined by the logarithm of the frequency, *e.g.* $4 = 10^4$ Hz.

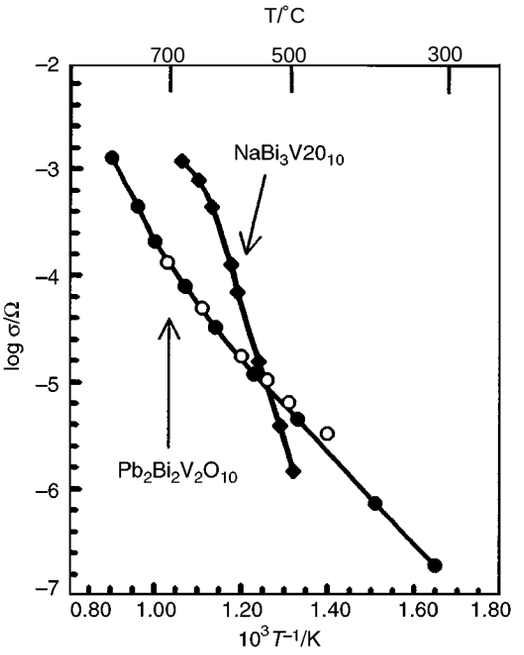

Fig. 4 Arrhenius plots of bulk conductivity in air. Open and closed circles represent heating and cooling data for $Pb_2Bi_2V_2O_{10}$, respectively. Filled squares correspond to data for $NaBi_3V_2O_{10}$.[8]

plot, Fig. 4. Reported data for $NaBi_3V_2O_{10}$ are included for comparison. The Arrhenius plot for $Pb_2Bi_2V_2O_{10}$ shows significant curvature, especially above *ca.* 600 °C, however there is no abrupt change in slope as observed for $NaBi_3V_2O_{10}$, Fig. 4, suggesting that $Pb_2Bi_2V_2O_{10}$ melts before any phase transition to a higher symmetry polymorph can occur. The absence of any structural phase transition was supported by differential thermal analysis on a powdered sample of $Pb_2Bi_2V_2O_{10}$ between 25 and 850 °C and is in agreement with the results of Brixner and Foris.[10] Below *ca.* 600 °C a linear response is observed with an associated activation energy of 0.8 eV. This conductivity behaviour is in contrast to that observed for $NaBi_3V_2O_{10}$, which exhibits a rapid rise in conductivity up to the phase transition temperature at *ca.* 575 °C, before approaching a limiting value of *ca.* 1 mS cm^{-1} prior to decomposition at *ca.* 700 °C, Fig. 4. Thus, although $NaBi_3V_2O_{10}$ and $Pb_2Bi_2V_2O_{10}$ are isostructural at room temperature they exhibit contrasting conductivity behaviour.

In summary, $NaBi_3V_2O_{10}$ and $Pb_2Bi_2V_2O_{10}$ have triclinic symmetry at room temperature which is presumably a result of structural distortions associated with lone electron pairs on Bi^{+III} and Pb^{+II} ions. Electrical measurements suggest that both phases are modest oxide ion conductors and that $Pb_2Bi_2V_2O_{10}$ melts without undergoing a structural transformation to some higher symmetry polymorph. In contrast, $NaBi_3V_2O_{10}$ undergoes a reversible phase transition at *ca.* 575 °C. As Na ions do not have any lone electron pairs, replacement of Pb^{+II} by Bi^{+III} and Na^{+I} may reduce structural distortions associated with the lone electron pairs in $NaBi_3V_2O_{10}$ and therefore facilitate structural transformation to a higher symmetry polymorph with enhanced conductivity.

Acknowledgements

We thank Dr Alison Coats for EPMA analysis, Dr Karl Ryder for ESR measurements, EPSRC for a studentship (EM) and use of the Chemical Database Service at Daresbury and Dr Ron Smith (Rutherford Appleton Laboratory) for assistance with collection of neutron diffraction data.

References

1 T. Takahashi and H. Iwahara, *Mater. Res. Bull.*, 1978, **13**, 1447.
2 F. Abraham, J. C. Boivin, G. Mairesse and G. Nowogrocki, *Solid State Ionics*, 1990, **40/41**, 934.
3 T. Lu and B. C. H. Steele, *Solid State Ionics*, 1986, **21**, 339.
4 P. Wood, D. C. Sinclair and F. P. Glasser, *Solid State Ionics*, 1993, **66**, 151.
5 G. Pang, S. Feng, Y. Tang, C. Tan and R. Xu, *Chem. Mater.*, 1998, **10**, 2446.
6 W. J. Zhou, *J. Solid State Chem.*, 1990, **87**, 44.
7 W. J. Zhou, PhD Thesis, University of Cambridge, 1987.
8 D. C. Sinclair, C. J. Watson, R. A. Howie, J. M. S. Skakle, A. M. Coats, C. A. Kirk, E. E. Lachowski and J. Marr, *J. Mater. Chem.*, 1998, **8**, 281.
9 D. A Fletcher, R. F. McMeeking and D. J. Parkin, *Inf. Comput. Sci.*, 1996, **36**, 746.
10 L. H. Brixner and C. M. Foris, *Mater. Res. Bull.*, 1974, **9**, 273.
11 P. L. Wang and D. Y. Li, *Acta Phys. Sin.*, 1985, **34**, 235.
12 B. F. Mentzen, A. Latrach, J. Bouix and A. W. Hewat, *Mater. Res. Bull.*, 1984, **19**, 549.
13 P. Y. Lui, MSc Thesis, University of Aberdeen, 1998.
14 R. I. Smith and S. Hull, Report RAL-TR-97-038, Rutherford Appleton Laboratory, 1997.
15 W. I. F. David, R. M. Ibberson and J. C. Mathewman, Report RAL-92-032, Rutherford Appleton Laboratory, 1992.
16 V. F. Sears, *Neutron News*, 1992, **3**, 26.
17 I. D. Brown and D. Altermatt, *Acta Crystallogr., Sect. B*, 1985, **41**, 244.
18 J. T. S. Irvine, D. C. Sinclair and A. R. West, *Adv. Mater.*, 1990, **2**, 132.

Paper 9/04273C